# An Improved Transistor Modeling Methodology Exploiting the Quasi-Static Approximation

ANWAR JARNDAL [1], GIOVANNI CRUPI [2], ANTONIO RAFFO[3], VALERIA VADALÀ [3],
AND GIORGIO VANNINI[3]

1 Department of Electrical Engineering, University of Sharjah, Sharjah, UAE
2 Department of Biomedical and Dental Sciences and Morphofunctional Imaging, University of Messina, 98122 Messina, Italy
3 Department of Engineering, University of Ferrara, 44121 Ferrara, Italy

CORRESPONDING AUTHOR: A. JARNDAL (e-mail: ajarndal@sharjah.ac.ae)
This work was supported by the University of Sharjah, UAE.

**ABSTRACT** In this paper, a new modeling technique is proposed for extracting small-signal lumped-element equivalent-circuit models for microwave transistors. The proposed procedure is based on using an optimization approach that is improved by targeting a quasi-static behavior as additional objective function rather than only minimizing the error between the simulated and measured scattering parameters. The validity of the developed modeling methodology is successfully demonstrated by considering a 0.25x1000 $\mu m^2$ gallium nitride (GaN) high-electron-mobility transistor (HEMT) as a case study.

**INDEX TERMS** GaN HEMT, non-quasi-static effects, scattering parameter measurements, semiconductor device modeling, silicon carbide substrate.

## I. INTRODUCTION

The small-signal lumped-element equivalent-circuit modeling of microwave transistors has been much debated and is still being debated [1]–[8], since this area of research is of great interest but also very challenging. The large interest comes mostly from the fact that the small-signal lumped-element equivalent-circuit models often act as foundation for large-signal and noise modeling [9]–[15]. However, small-signal lumped-element equivalent-circuit modeling becomes more and more challenging due to the continuous increase in transistor operating frequencies and gate width enlargement, in order to enable higher-frequency and higher-power applications. The onset of the distributed effects [16], [17] and non-quasi-static (NQS) effects [18], [19] make the model extraction much more critical. Over the years, optimization-based model identification has demonstrated to be a powerful modeling tool to accomplish this critical task [20]–[23].

As well known, the local minima are typical problems with this deterministic method, especially for local approaches including gradient and simplex methods [24]. The optimization process could stack in a local minimum instead of attaining the global solution and thus physical non-relevant values could be obtained [3]. The performance depends on the initial guess and thus many techniques have been reported to address this problem. One of these techniques is the hybrid approach based on combining the optimization and direct methods [23]. The direct method could be used to initiate the extraction process by generating reliable estimation for the equivalent-circuit elements, which would then be used as an appropriate starting point for the local optimization process [23]. The reliability of the initial and thus the final values depends on the base measurements. The direct extraction procedure can be critically sensitive to the measurement uncertainty, which is less critical for the optimization methods.

In this paper, the proposed optimization-based modeling methodology deals with the local minima problem by using the global optimization approach instead of the local one. The global optimization techniques are based on the multiple-point initialization instead of the single starting point used in the local methods. In addition, these points are randomly generated to cover the whole search space and thus to avoid the initial guess dependency. In general, these techniques have no local minima problem. The efficiency of the global techniques to find the global optimum values depends on their exploration and exploitation capability [25]. Some of these global optimization methods, such as particle

swarm optimization (PSO) [26], have stronger exploitation and thus they are faster with higher rate of convergence. However, the PSO exploration is poor and thus could get stuck in local minima, especially for a large-scale problem with higher number of variables [27]. On the other side, the genetic algorithm (GA) optimization approach has stronger exploration capability and thus it can be used for complicated problems [28]. Other global optimization techniques, such as artificial bee colony (ABC), are in between with respect to PSO and GA [29]–[31]. The targeted global optimum (best solution) is interrelated to the objective function definition. This could be restricted to be the error function between the measured and simulated data. In this case, the extraction process will target the model accuracy to find the best fitting. However, this could not guarantee the reliability of the extracted values.

In this paper, the critical problem of the model parameter reliability is successfully addressed by developing a new approach based on targeting quasi-static behavior as an additional objective function. This is because the NQS effects can be disregarded at relatively low frequencies, since they represent the inertia of the intrinsic transistor in responding to rapid voltage changes and thus, they become more evident with increasing frequency. As a matter of fact, at different parasitic networks correspond different intrinsic descriptions; the capability of guaranteeing the intrinsic quasi-static behavior at higher frequencies definitely represents an added value for the model. In fact, it is worth mentioning that NQS effects [32]–[34] are quite complex to model and do not scale with device periphery, so an intrinsic model for which NQS effects appear prematurely is inherently less accurate and scalable. The proposed technique has been validated by using a 0.25x1000 $\mu m^2$ GaN HEMT on SiC substrate but can be applicable to other types of field-effect transistors (FETs), since this approach is technology-independent.

This paper is structured as follows. The device-under-test and the experiments are described in Section II, two different model topologies are presented in Section III, the developed optimization-based modeling techniques and results are discussed in Section IV, the modified techniques and the achieved improvements are presented in Section V, and finally, conclusions are given in Section VI.

## II. DEVICE UNDER TEST AND CHARACTERIZATION
The analyzed device is an on-wafer interdigitated HEMT based on an AlGaN/GaN heterostructure grown on SiC substrate. This device has a gate length of 0.25 $\mu m$ and a gate width of 8x125 $\mu m$. The fabrication process is the GH25-10 technology by United Monolithic Semiconductors (UMS) [35]. Table 1 shows the maximum ratings for this technology whereas Fig. 1(a) shows a picture of the characterized device.

Y-parameter measurements for the device at "cold" pinch-off bias condition ($V_{GS} = -3$ V and $V_{DS} = 0$ V) are presented in Fig. 1(b). The evidence of parasitic effects is clear from the two resonances in the measured input and

**TABLE 1.** Maximum ratings for 8x125-$\mu$m HEMT device.

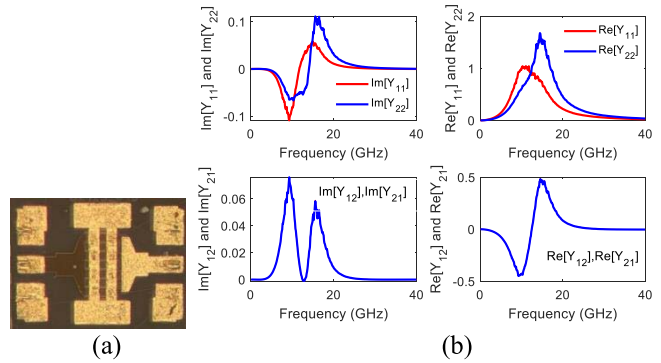| Parameter | Unit | Recommended | Maximum |
|---|---|---|---|
| Drain-Source Biasing Voltage @120 mA/mm | V | 30 | 55 |
| Gate-Source Voltage | V | -20 | -25 |
| Drain-Gate Voltage | V | 80 | 120 |
| Gate current | mA/finger | 2 | 60 |
| ft | GHz | 30 | - |
| fmax | GHz | > 50 | - |



**FIGURE 1.** (a) Picture of a 0.25x1000 $\mu m^2$ GaN HEMT used during the experimental characterization. (b) Y-parameter measurements of a 0.25x1000 $\mu m^2$ GaN HEMT at the "cold" pinch-off condition ($V_{GS} = -3$ V and $V_{DS} = 0$ V).

output impedances $Y_{11}$ and $Y_{22}$. The $1^{st}$ resonance is due to the interaction between the shunt capacitances and series inductances, while the $2^{nd}$ resonance around 15 GHz is due to the influence of series resistances.

## III. EQUIVALENT CIRCUIT MODEL
Two small-signal models are investigated (see Fig. 2). The first model in Fig. 2(a) is the standard one that considers only the pad capacitances, while the other interconnection capacitances are absorbed in the intrinsic capacitances. Frequency range up to 15 GHz was used for extracting the extrinsic elements of the model. Higher frequency range could stimulate extra distributed capacitive parasitic effects and in this case, the other model in Fig. 2(b) has to be implemented. In this extended model, the additional elements $C_{gsi}$, $C_{dsi}$, and $C_{gdi}$ are meant to consider the impact of the finger interconnection capacitances, which becomes more evident at high frequency.

## IV. OPTIMIZATION-BASED METHOD
The optimization-based extraction approach was developed and applied to the considered 1-mm GaN HEMT on SiC substrate. Three different optimization techniques were investigated: PSO, GA, and ABC. The following three subsections introduce the proposed procedures and their extraction results.

### A. PSO OPTIMIZATION-BASED METHOD
As well, know, the PSO optimization is based on initializing a population of candidate solutions, called swarm of

particles [26]. These particles move within the search-space according to mathematical formulas. Their movements over the entire search-space are guided by their local and global best positions. The values of these parameters are updated at each movement of the swarm and the process is repeated till the best position (solution) is found. As illustrated in Fig. 3, our PSO-based extraction procedure starts by using an initial population of 200 candidate solutions. S-parameters at "cold" pinch-off condition ($V_{GS} = -3$ V and $V_{DS} = 0$ V) are used to find lower/upper boundaries for the extrinsic capacitances; while S-parameters at unbiased condition ($V_{GS} = 0$ V and $V_{DS} = 0$ V) are used to estimate lower/upper boundaries for the extrinsic inductances and resistances. The maximum number of iterations is fixed at 100; however, the program has another termination criterion, which is the relative error whose minimum value has been fixed at $10^{-5}$. The relative error is monitored during the optimization process. If the relative error is almost constant over 25 iterations (no further reduction for the error), then the optimization process will be stopped. The small-signal model elements are optimized to minimize the error (maximize the fitness) between the simulated and measured S-parameters at the "cold" pinch-off condition. The error is defined as follows:

$$\varepsilon_r = \frac{1}{N} \left\| \sum_{n=1}^{N} \sum_{\substack{i=1,2 \\ j=1,2}} \left[ \left( Re\left( S_{ij,n}^m - S_{ij,n}^p \right) \right)^2 \right. \right.$$
$$\left. \left. + \left( Im\left( S_{ij,n}^m - S_{ij,n}^p \right) \right)^2 \right] \frac{1}{W_{ij}} \right\| \quad (1)$$

where $N$ is the total number of the considered frequency points and $S^m$ and $S^p$ are the measured and simulated S-parameters, respectively. $W_{ij}$ is a weighting factor used to de-emphasise data points that show high uncertainty. The impact of measurement uncertainty increases in the data regions with high reflection and/or low transmission coefficient [36]. The procedure was implemented in MATLAB and applied to both models [see Figs. 2(a) and 2(b)]. A computer with 1.9 GHz Core-i7 processor and 16 GB RAM was used. The extraction results are listed in Table 2 for the standard model and in Table 3 for the extended one. In the same tables, information about the minimum error, number of iterations, and the execution time are also reported. Fig. 4 shows the comparison between measurements and model simulations at "cold" pinch-off condition for the frequency range going from 0.1 to 15 GHz.

As can be noted, at this frequency range the standard model cannot efficiently characterize the contributions of the parasitic capacitances. This could be observed from the overestimated values of the intrinsic capacitances in Table 2. Typically, the intrinsic and extrinsic capacitances have comparable values for "cold" pinched-off devices [8]. The extended model is able to provide a more realistic



(a)



(b)
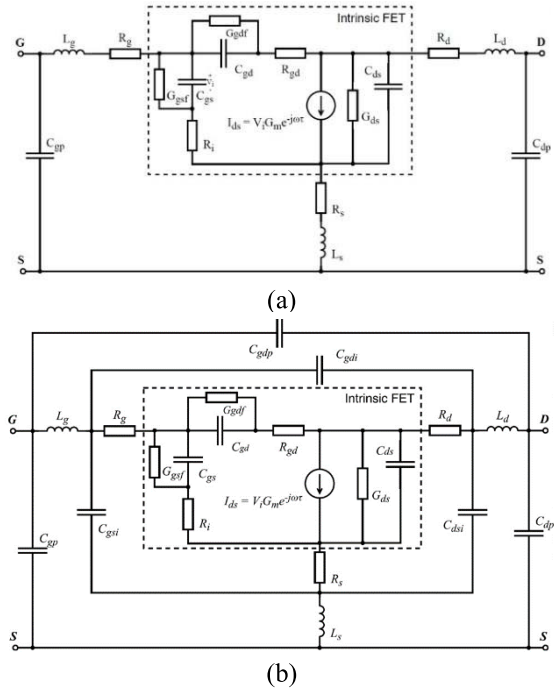
**FIGURE 2.** Small-signal lumped-element equivalent-circuit models: (a) the standard and (b) the extended configurations.
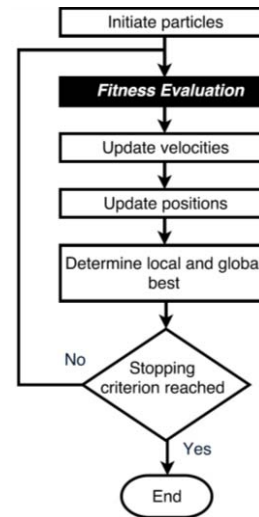


**FIGURE 3.** Flow chart for the PSO-based extraction procedure.

estimation of the intrinsic capacitances. However, the extraction procedure fails to provide reliable distribution for the extrinsic capacitance between the pad and inter-connection capacitances. This is clear from the zero values of the pad capacitances $C_{gp}$, $C_{dp}$ and $C_{gdp}$ in Table 3. As shown in Fig. 4, the simulation results confirm our observation of higher accuracy of the extended model at this frequency range with respect to the standard one. However, as it is well known, the reliability of the model extraction is not guaranteed with conventional error-based optimization methods. The targeted error function in equation (1) relies only on the fitting of the measurements, which could be achieved even
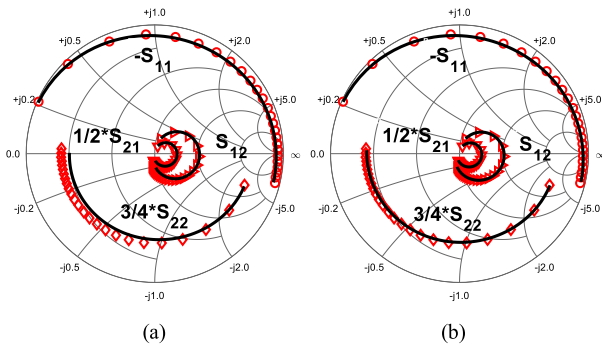
**FIGURE 4.** Comparison between (symbols) measurements at the "cold" pinch-off condition ($V_{GS} = -3$ V, $V_{DS} = 0$ V) and (lines) simulations based on using the PSO optimization applied to: (a) the standard model and (b) the extended one. The frequency range goes from 0.1 to 15 GHz.

**TABLE 2.** Extracted circuit elements, minimum error, number of iterations, and execution time for the standard model for the 1-mm GaN on SiC HEMT at the "cold" pinch-off bias condition ($V_{GS} = -3$ V and $V_{DS} = 0$ V) using PSO-, GA-, and ABC-based methods.

| Model Element | PSO | GA | ABC |
|---|---|---|---|
| $C_{gs}$ (fF) | 908.4 | 888 | 900.5 |
| $C_{gd}$ (fF) | 438.5 | 426 | 427 |
| $C_{ds}$ (fF) | 624.2 | 613 | 638.5 |
| $R_g$ (Ω) | 0.46 | 0.45 | 0.47 |
| $R_d$ (Ω) | 2.11 | 2.14 | 2.15 |
| $R_s$ (Ω) | 0.64 | 0.54 | 0.66 |
| $L_g$ (pH) | 148.8 | 151 | 151.5 |
| $L_d$ (pH) | 115 | 116 | 116 |
| $L_s$ (pH) | 8.0 | 7.9 | 8.4 |
| $C_{gp}$ (fF) | 67.5 | 95 | 6.4 |
| $C_{dp}$ (fF) | 81.6 | 74 | 64.7 |
| Error | 1.23 e-01 | 1.7 e-02 | 1.22 e-01 |
| No. of Iterations | 29 | 60 | 54 |
| Time (s) | 160 | 480 | 451 |

with zero values for some model elements, as we have seen in Table 3.

## B. GA OPTIMIZATION-BASED METHOD

The same procedure has been repeated using genetic algorithm optimization and applied to both the standard and extended models. GA has extra steps with respect to PSO. These include additional crossing (reproduction) and mutation processes, which significantly improve the exploration capability of the GA [28]. Fig. 5 presents the implemented GA-based extraction method. The same objective function in equation (1) was targeted.

Here, the number of initial populations is increased to 1000, which is recommended for this kind of optimization [37]. The other two parameters, namely the maximum number of iterations and the minimum relative error, are kept as they were for the PSO procedure. The results of the GA procedure for the standard and extended models are listed in Tables 2 and 3, respectively. As expected, the execution time is longer than for PSO and this is due

**TABLE 3.** Extracted circuit elements, minimum error, number of iterations, and execution time for the extended model for the 1-mm GaN on SiC HEMT at the "cold" pinch-off bias condition ($V_{GS} = -3$ V and $V_{DS} = 0$ V) using PSO-, GA-, and ABC-based methods.

| Model Element | PSO | GA | ABC |
|---|---|---|---|
| $C_{gs}$ (fF) | 110.2 | 90.1 | 103 |
| $C_{gd}$ (fF) | 417.4 | 298.5 | 355.2 |
| $C_{ds}$ (fF) | 218.9 | 55.1 | 193.6 |
| $R_g$ (Ω) | 2.34 | 3.44 | 2.83 |
| $R_d$ (Ω) | 1.81 | 1.99 | 1.88 |
| $R_s$ (Ω) | 1.19 | 0.97 | 1.07 |
| $L_g$ (pH) | 151.7 | 151.7 | 151.8 |
| $L_d$ (pH) | 120.1 | 120.1 | 119.4 |
| $L_s$ (pH) | 8.6 | 8.6 | 8.55 |
| $C_{gp}$ (fF) | 0.0 | 0.0 | 0.0 |
| $C_{dp}$ (fF) | 0.0 | 2.0 | 9.8 |
| $C_{gdp}$ (fF) | 0.0 | 0.0 | 0.0 |
| $C_{gsi}$ (fF) | 833.1 | 859.4 | 840 |
| $C_{dsi}$ (fF) | 457 | 620 | 478 |
| $C_{gdi}$ (fF) | 0.0 | 122 | 64.9 |
| Error | 2.2 e-02 | 1.71 e-02 | 2.19 e-02 |
| No. of Iterations | 44 | 60 | 100 |
| Time (s) | 230 | 480 | 733 |
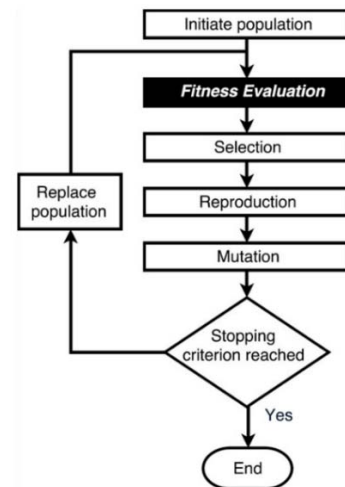


**FIGURE 5.** Flow chart for the GA-based extraction procedure.

to the mentioned extra operations of crossing and mutation. The extracted values are nearly equal to the ones obtained using PSO. Fig. 6 shows the model simulations at "cold" pinch-off condition ($V_{GS} = -3$ V and $V_{DS} = 0$ V).

As can be noted, both PSO and GA approaches provide almost the same accuracy with similarly low reliability. The cost of using PSO for this small-scale problem is lower than GA with lower number of iterations and faster process. For larger-scale problem, the GA outperform the PSO [37] and this is clear from the obtained value of $C_{gdi}$ with respect to the zero-value using PSO.

## C. ABC OPTIMIZATION-BASED METHOD

For further investigation, the ABC-based optimization has been applied also to both the standard and extended models.
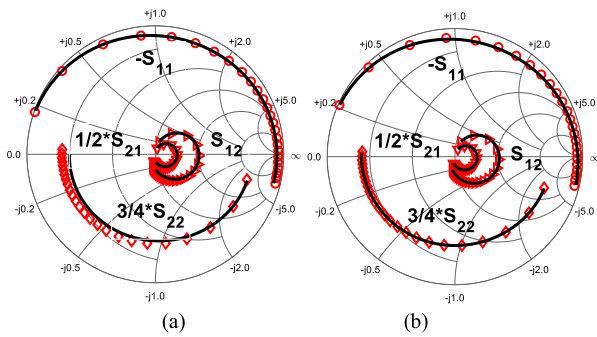
**FIGURE 6.** Comparison between (symbols) measurements at the "cold" pinch-off condition ($V_{GS} = -3$ V, $V_{DS} = 0$ V) and (lines) simulations based on using the GA optimization applied to: (a) the standard model and (b) the extended one. The frequency range goes from 0.1 to 15 GHz.

Both PSO and ABC are swarm intelligent methods, and they start by generating initial candidate solutions to explore the whole search-space and then, by utilizing mathematical operators, to exploit and produce new solutions [29]. As was mentioned, in case of PSO the updated movements (velocity) and positions provide new solutions. In case of ABC, the whole swarm is subdivided into three groups of bees: scout, employed, and onlooker bees. The scouts randomly generate solutions (exploration), while the onlooker and employed are responsible for their selection and updating (exploitation), respectively [30]. The employed bees produce new solutions based on the information from the scout and onlooker bees. The ABC extraction procedure is illustrated by the flow chart in Fig. 7.

The complexity of this technique is in between the PSO and GA procedures. Here only the initial population was changed to be 500, which could be enough for this case. The same objective function in equation (1) was targeted. As can be seen from the listed results in Tables 2 and 3, this technique provides nearly similar values to the ones obtained using the PSO and GA procedures. Fig. 8 presents a comparison between the measured and simulated "cold" pinch-off S-parameters. As can be seen, the performance of the ABC technique is in between the PSO and GA procedures.

For the standard model with smaller number of variables, GA and ABC have the same performance with same rate of convergence and speed of processing. For the extended model with larger number of elements, GA outperforms ABC, and this could be noted from the lower rate of convergence and longer execution time of the latter. This observation has been reported in [31], which confirms better performance of GA in case of larger size problem having a higher number of optimization variables.

In general, the reliability of parameter extraction could be investigated by comparing the intrinsic capacitances with the pad capacitances. This could be assessed also by the non-zero values of the model elements. Typically, under "cold" pinch-off, the intrinsic capacitances, such as $C_{gs}$, show values comparable to the total extrinsic capacitances [8]. The extraction results using all three techniques show unreliable
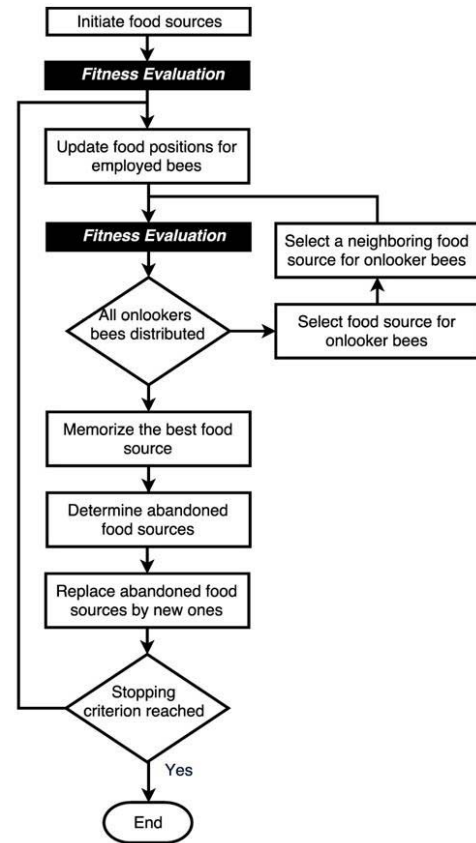


**FIGURE 7.** Flow chart for the ABC-based extraction procedure.
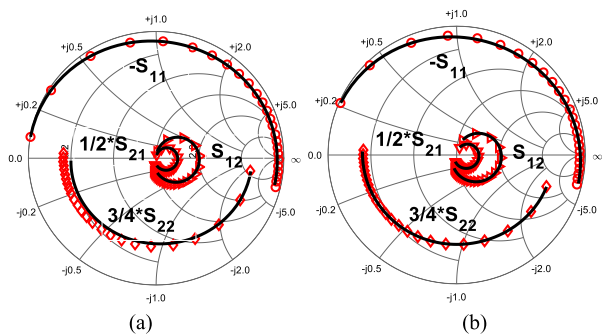


**FIGURE 8.** Comparison between (symbols) measurements at the "cold" pinch-off condition ($V_{GS} = -3$ V, $V_{DS} = 0$ V) and (lines) simulations based on using the ABC optimization applied to: (a) the standard model and (b) the extended one. The frequency range goes from 0.1 to 15 GHz.

distribution for the total capacitances between $C_{gs}$ ($\approx 0.9$ pF) and $C_{pg}$ ($\approx 0.1$ pF) for the case of the standard model. In case of the extended model, all techniques show non reliable zero values for the pad and inter-electrode capacitances. All techniques target the minimum error between the measured and simulated S-parameters. Here it is clear that targeting only the fitting error is not enough to provide reliable extraction results.

The model identification procedures have been also evaluated in terms of their reliability when de-embedding the

**TABLE 4.** Extracted intrinsic elements of lumped and extended models for 1-mm GaN on SiC HEMT at active bias condition of $V_{GS} = -1$ V and $V_{DS} = 12.5$ V using PSO-based method.
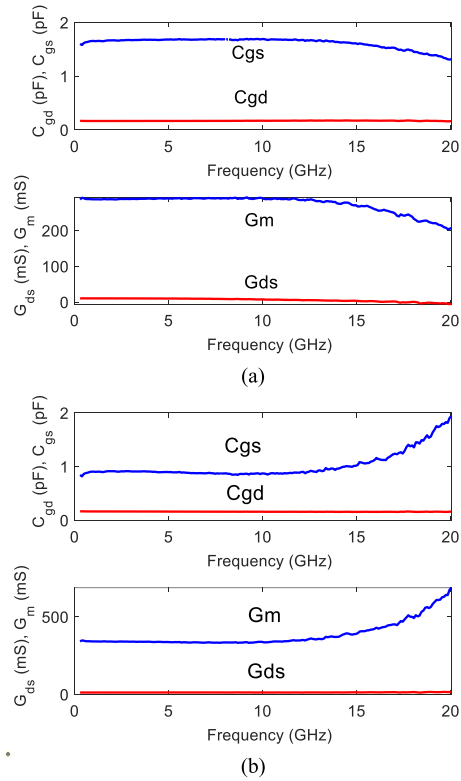
| Model Element | Standard Model | Extended Model |
|---|---|---|
| $C_{gs}$ (fF) | 1700 | 892 |
| $C_{gd}$ (fF) | 169 | 162 |
| $C_{ds}$ (fF) | 732 | 138 |
| $R_i$ (Ω) | 0.38 | 9.55 |
| $R_{gd}$ (Ω) | 33.6 | 12.3 |
| $G_m$ (mS) | 292 | 336.6 |
| $G_{ds}$ (mS) | 10.6 | 12.6 |
| $\tau$ (ps) | 0.0 | 3.95 |
| $G_{gsF}$ (mS) | 0.04 | 0.05 |
| $G_{gdf}$ (mS) | 0.0 | 0.0 |
| Error | 1.11 e-01 | 2.25 e-01 |

extrinsic parasitic effects. The frequency dependency of the intrinsic elements is an indicator of parasitic effects, which may not have been properly removed. This might result in a gradual increase or decrease of the values of the intrinsic elements versus frequency. Fig. 9 shows the curves of intrinsic elements at the active bias condition of $V_{GS} = -1$ V and $V_{DS} = 12.5$ V, where the values were obtained after de-embedding the extrinsic elements in case of both standard and extended models. Here PSO-based extracted values are used but the same frequency-dependent effect is observed with GA and ABC-based ones. As can be seen, for both models the extraction procedure does not accurately characterize and then de-embed the parasitic effects. This of course will result in frequency dependency of the intrinsic part, which is violating the quasi-static assumption required for an accurate characterization of the intrinsic behavior of the transistor. The extracted intrinsic elements at this bias condition are listed in Table 4. The values of these elements are statistically averaged by means of linear regression [8]. The model accuracy is demonstrated by fitting the measured S-parameters at the same considered active bias condition and the obtained results are presented in Fig. 10. The optimization-based procedures have better performance with the standard model and this could be observed from its lower fitting error, with respect to the extended model (see Table 4).

## V. IMPROVED OPTIMIZATION-BASED METHOD

The same optimization procedures have been repeated with an improved formulation for the objective function. Here, the quasi-static behavior of the intrinsic transistor has been targeted in addition to the fitting error. Thus, the error objective function in equation (1) is extended by adding the normalized standard deviation of the intrinsic elements at typical active operating bias conditions on a $50 - \Omega$ dynamic load line (see Fig. 11). The lower frequency-dependence (deviation) of the intrinsic parameters is a measure for accuracy on characterizing and de-embedding the device parasitic effects. The error function is defined as:

$$\varepsilon = \varepsilon_r + k_1\sigma_{Cgs} + k_2\sigma_{Cgd} + k_3\sigma_{Cds} + k_4\sigma_{Gm} \quad (2)$$



**FIGURE 9.** Intrinsic elements versus frequency for a 1-mm GaN on SiC HEMT at the active bias condition of $V_{GS} = -1$ V and $V_{DS} = 12.5$ V using PSO-based method applied to: (a) the standard model and (b) the extended one.
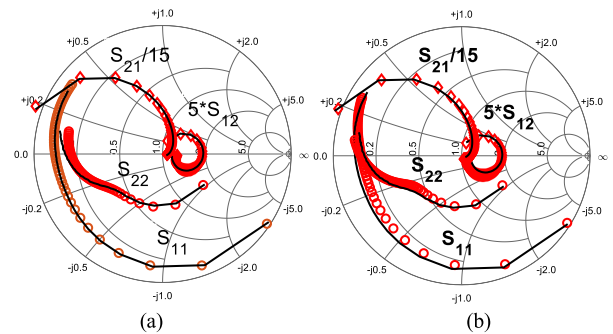


**FIGURE 10.** Comparison between (symbols) measurements at the active bias condition of $V_{GS} = -1$ V, $V_{DS} = 12.5$ V and (lines) simulations based on using the PSO optimization applied to: (a) the standard model and (b) the extended one. The frequency range goes from 0.1 to 20 GHz.

where, $\sigma_{Cgs}$, $\sigma_{Cgd}$, $\sigma_{Cds}$, and $\sigma_{Gm}$ are the normalized mean standard deviations of $C_{gs}$, $C_{gd}$, $C_{ds}$, and $G_m$, respectively, at different bias conditions and $\varepsilon_r$ is the original error function in (1).

Typical bias conditions of A, AB, and B classes of operation were included (see Fig. 11) and thus, $\sigma_{Cgs}, \sigma_{Cgd}, \sigma_{Cds}$, *and* $\sigma_{Gm}$ are calculated as follows:

$$\sigma_{Cgs} = \sqrt{\frac{1}{3}\left[\left(\frac{\sigma_{Cgs,A}}{\mu_{Cgs,A}}\right)^2 + \left(\frac{\sigma_{Cgs,AB}}{\mu_{Cgs,AB}}\right)^2 + \left(\frac{\sigma_{Cgs,B}}{\mu_{Cgs,B}}\right)^2\right]} \quad (3)$$
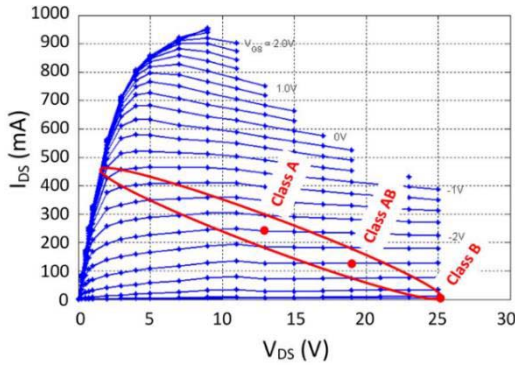
**FIGURE 11.** Illustration of three typical active operating bias conditions on (red) a 50-Ω dynamic load line in conjunction with (blue) the measured DC IV characteristics of the studied 0.25x1000 $\mu m^2$ GaN HEMT on SiC substrate.

$$\sigma_{Cgd} = \sqrt{\frac{1}{3}\left[\left(\frac{\sigma_{Cgd,A}}{\mu_{Cgd,A}}\right)^2 + \left(\frac{\sigma_{Cgd,AB}}{\mu_{Cgd,AB}}\right)^2 + \left(\frac{\sigma_{Cgd,B}}{\mu_{Cgd,B}}\right)^2\right]} \quad (4)$$

$$\sigma_{Cds} = \sqrt{\frac{1}{3}\left[\left(\frac{\sigma_{Cds,A}}{\mu_{Cds,A}}\right)^2 + \left(\frac{\sigma_{Cds,AB}}{\mu_{Cds,AB}}\right)^2 + \left(\frac{\sigma_{Cds,B}}{\mu_{Cds,B}}\right)^2\right]} \quad (5)$$

$$\sigma_{Gm} = \sqrt{\frac{1}{3}\left[\left(\frac{\sigma_{Gm,A}}{\mu_{Gm,A}}\right)^2 + \left(\frac{\sigma_{Gm,AB}}{\mu_{Gm,AB}}\right)^2 + \left(\frac{\sigma_{Gm,B}}{\mu_{Gm,B}}\right)^2\right]} \quad (6)$$

where $\sigma$ and $\mu$ are the standard deviation and mean values of the intrinsic element, respectively. $k_1$, $k_2$, $k_3$, and $k_4$ in (2) are experimentally found scaling factors to insure proper weighted summation for the error and the standard deviations. Initially, the optimization process is started by just including $\varepsilon_r$ to monitor its range. Then, the scaling factors are selected to have the same range of $\varepsilon_r$ and the process is reaped to minimize the whole error $\varepsilon$ defined by (2). The results of the model extractions with the modified objective function for the three optimization techniques are listed in Tables 5 and 6 for the standard and extended models, respectively. The extraction results for the standard model are similar to the previously extracted ones and listed in Table 2. Adding more restrictions to the objective function did not provide further improvement for the model accuracy. The reliability of extraction has not been improved either and this could be attributed to the simplicity of the model topology. However, it is interesting to see that the rate of convergence for both GA and ABC was improved with the modified objective function. This could be observed from the shorter execution times in Table 5 with respect to the presented values in Table 2. This could be attributed to the multi-objective formulation of the error function, which, as it was reported in [38], improves the rate of convergence. For this multi-finger device with a large size periphery, the standard model cannot provide reliable modeling even with improved formulation of the error function. This justification is supported by the results in Table 6 for the extended model.

**TABLE 5.** Extracted circuit elements, minimum error, number of iterations, and execution time for the standard model for the 1-mm GaN on SiC HEMT at the "cold" pinch-off bias condition ($V_{GS} = -3$ V and $V_{DS} = 0$ V) using improved PSO-, GA-, and ABC-based methods.

| Model Element | Mod. PSO | Mod. GA | Mod. ABC |
|---|---|---|---|
| $C_{gs}$ (fF) | 908 | 907.9 | 908 |
| $C_{gd}$ (fF) | 439.5 | 439.5 | 439.5 |
| $C_{ds}$ (fF) | 622 | 622 | 622 |
| $R_g$ (Ω) | 0.47 | 0.47 | 0.47 |
| $R_d$ (Ω) | 2.1 | 2.1 | 2.1 |
| $R_s$ (Ω) | 0.63 | 0.63 | 0.63 |
| $L_g$ (pH) | 148.8 | 148.8 | 148.8 |
| $L_d$ (pH) | 114.7 | 114.7 | 114.7 |
| $L_s$ (pH) | 8.0 | 8.0 | 8.0 |
| $C_{gp}$ (fF) | 66.7 | 66.6 | 66.7 |
| $C_{dp}$ (fF) | 86.4 | 87.0 | 86.9 |
| Error | 1.39 e-01 | 1.39 e-01 | 1.39 e-01 |
| No. of Iterations | 39 | 27 | 27 |
| Time (s) | 302 | 245 | 292 |
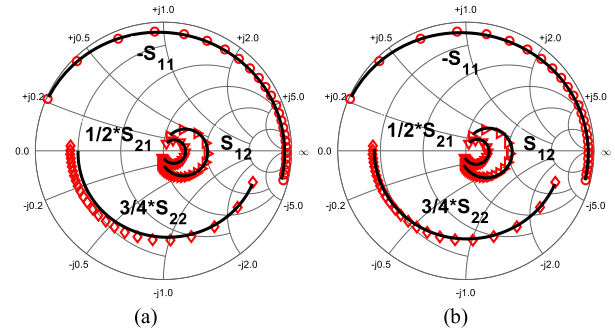


**FIGURE 12.** Comparison between (symbols) measurements at the "cold" pinch-off condition ($V_{GS} = -3$ V, $V_{DS} = 0$ V) and (lines) simulations based on using the improved PSO optimization applied to: (a) the standard model and (b) the extended one. The frequency range goes from 0.1 to 15 GHz.

The optimization procedures with the improved error function work definitely well with the extended model. This could be observed from the non-zero values of the inter-electrode capacitances $C_{gsi}$, $C_{dsi}$, and $C_{gdi}$. Their values are also realistic to reflect their stronger impact for this device of ten inter-connected fingers. The value of $C_{dsi}$ with respect to $C_{gsi}$ is higher and this of course is because of the wider area of the drain manifold. This improved model procedure showed more accurate fitting for the measurements (see Figs. 12–14) and lower error (see Table 6) with respect to the listed fitting error in Table 3.

The optimization-based procedure with modified objective function has been also validated in terms of the reliable modeling under active bias condition. The extrinsic elements for both models have been de-embedded to access the intrinsic part of the device. Then, the intrinsic elements are extracted by means of curve fitting. Fig. 15 shows intrinsic elements versus frequency for both models.

There is no further improvement for the standard model because of almost the same extrinsic elements. Instead,
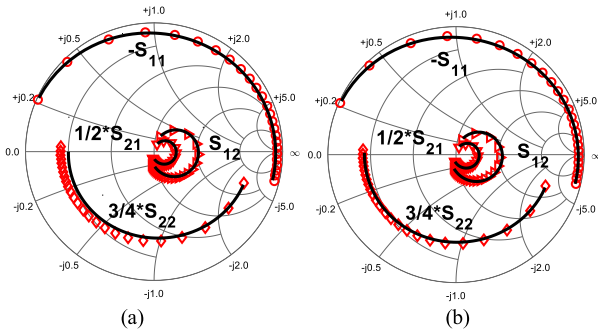
**FIGURE 13.** Comparison between (symbols) measurements at the "cold" pinch-off condition ($V_{GS} = -3$ V, $V_{DS} = 0$ V) and (lines) simulations based on using the modified GA optimization applied to: (a) the standard model and (b) the extended one. The frequency range goes from 0.1 to 15 GHz.

**TABLE 6.** Extracted circuit elements, minimum error, number of iterations, and execution time for the extended model for the 1-mm GaN on SiC HEMT at the "cold" pinch-off bias condition ($V_{GS} = -3$ V and $V_{DS} = 0$ V) using improved PSO-, GA-, and ABC-based methods.

| Model Element | Mod. PSO | Mod. GA | Mod. ABC |
|---|---|---|---|
| $C_{gs}$ (fF) | 672 | 591 | 672 |
| $C_{gd}$ (fF) | 414 | 381 | 414 |
| $C_{ds}$ (fF) | 282 | 295.1 | 282 |
| $R_g$ (Ω) | 0.72 | 0.91 | 0.74 |
| $R_d$ (Ω) | 2.1 | 2.1 | 2.1 |
| $R_s$ (Ω) | 0.74 | 0.73 | 0.74 |
| $L_g$ (pH) | 148 | 148.5 | 148.4 |
| $L_d$ (pH) | 116 | 116.2 | 116.2 |
| $L_s$ (pH) | 8.9 | 8.9 | 8.9 |
| $C_{gp}$ (fF) | 49 | 50 | 49.0 |
| $C_{dp}$ (fF) | 34 | 34.3 | 34.6 |
| $C_{gdp}$(fF) | 22 | 21.8 | 21.8 |
| $C_{gsi}$ (fF) | 242 | 323.3 | 241.8 |
| $C_{dsi}$ (fF) | 372 | 359.1 | 372.1 |
| $C_{gdi}$(fF) | 22 | 55.3 | 21.8 |
| Error | 7.67 e-027 | 7.7 e-02 | 7.68 e-02 |
| No. of Iterations | 36 | 39 | 52 |
| Time (s) | 327 | 292 | 539 |
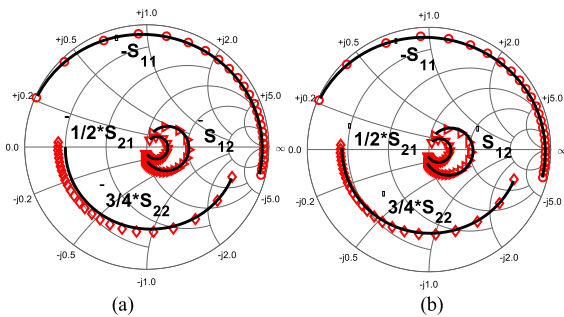


**FIGURE 14.** Comparison between (symbols) measurements at the "cold" pinch-off condition ($V_{GS} = -3$ V, $V_{DS} = 0$ V) and (lines) simulations based on using the modified ABC optimization applied to: (a) the standard model and (b) the extended one. The frequency range goes from 0.1 to 15 GHz.

there is a significant improvement for the extended model, which shows lower frequency dependency. This could be also observed from listed error in Tables 4 and 7. It means that the improved procedure is more efficient in characterizing

**TABLE 7.** Extracted intrinsic parameters of standard and extended models for the 1-mm GaN on SiC HEMT at active bias condition of $V_{GS} = -1$ V and $V_{DS} = 12.5$ V using the improved PSO procedure.

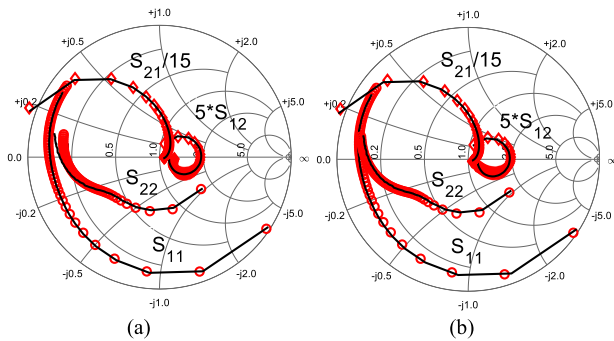| Model Element | Standard Model | Extended Model |
|---|---|---|
| Cgs (fF) | 1697 | 1489 |
| Cgd (fF) | 169 | 137 |
| Cds (fF) | 726 | 294 |
| Ri (Ω) | 0.4 | 1.68 |
| Rgd (Ω) | 33 | 17.5 |
| Gm (mS) | 291.9 | 298.1 |
| Gds (mS) | 10.5 | 10.8 |
| τ (ps) | 0 | 2.3 |
| Ggsf (mS) | 0.04 | 0.04 |
| Ggdf (mS) | 0.0 | 0.0 |
| Error | 1.1 e-01 | 1.61 e-01 |
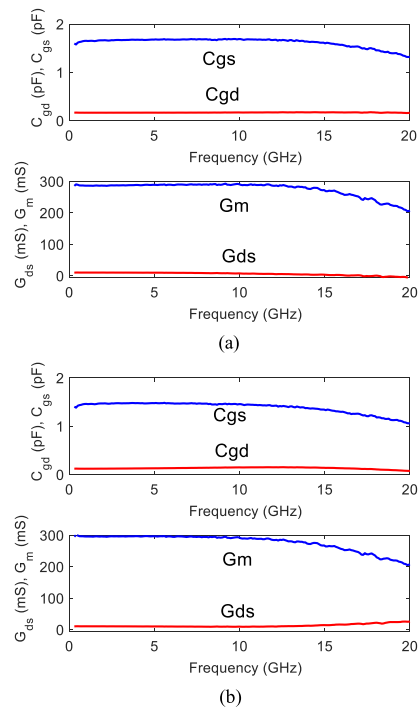


**FIGURE 15.** Intrinsic elements versus frequency for a 1-mm GaN on SiC HEMT at the active bias condition of $V_{GS} = -1$ V and $V_{DS} = 12.5$ V using modified PSO applied to: (a) the standard model and (b) the extended one.

and removing parasitic effects with respect to the standard error-fitting-based approach. As can be seen also in Fig. 16, a more accurate fitting with the measurements is obtained. This also noted from presented error in Tables 4 and 7. Table 7 lists extracted intrinsic elements at active bias condition in saturation region. The results are realistic and reflect the unsymmetrical capacitance distribution at this bias condition. Also, reliable values are obtained for $R_i$, $R_{gd}$ and $\tau$.

## VI. CONCLUSION
A reliable optimization method for small-signal equivalent-circuit model extraction has been theoretically developed and experimentally applied to the GaN HEMT technology. The

**FIGURE 16.** Comparison between (symbols) measurements at the active bias condition of $V_{GS} = -1$ V, $V_{DS} = 12.5$ V and (lines) simulations based on using the modified PSO optimization applied to: (a) the standard model and (b) the extended one. The frequency range goes from 0.1 to 20 GHz.

improvement of the proposed technique is achieved by targeting not only the maximization of the fitting with S-parameter measurements but also a quasi-static behavior of the intrinsic device as an objective function for parameter determination. This allows making the modeling results more reliable. As the modeling methodology is technology-independent, it can be applied to different types of FETs.

## REFERENCES

[1] J. A. Z. Flores and G. Kompa, "Closed-form extraction strategy of physically meaningful parameters of small-signal HEMT models with distributed parasitic capacitive effects," *IEEE Trans. Microw. Theory Techn.*, vol. 69, no. 2, pp. 1227–1237, Feb. 2021.

[2] S. Colangeli *et al.*, "Nondestructive, self-contained extraction method of parasitic resistances in HEMT devices," *IEEE Trans. Microw. Theory Techn.*, vol. 68, no. 7, pp. 2571–2578, Jul. 2020.

[3] G. Kompa, *Parameter Extraction and Complex Nonlinear Transistor Models*, Boston, MA, USA: Artech House, 2020.

[4] Z. Zhao *et al.*, "A fast small signal modeling method for GaN HEMTs," *Solid State Electron.*, vol. 175, Jan. 2021, Art. no. 107946.

[5] Z. Wen, Y. Xu, C. Wang, X. Zhao, and R. Xu, "An efficient parameter extraction method for GaN HEMT small-signal equivalent circuit model," *Int. J. Numer. Model. Electron. Devices Fields*, vol. 30, no. 1, Jan. 2017, Art. no. e2127.

[6] S. A. Ahsan, S. Ghosh, S. Khandelwal, and Y. S. Chauhan, "Physics-based multi-bias RF large-signal GaN HEMT modeling and parameter extraction flow," *IEEE J. Electron Devices Soc.*, vol. 5, no. 5, pp. 310–319, Sep. 2017.

[7] A. Jarndal and A. Kouki, "GaN high electron mobility transistors: A review from parasitic elements extraction's perspective," *J. Eng.*, vol. 2016, no. 7, pp. 258–265, Jul. 2016.

[8] A. Jarndal and G. Kompa, "A new small-signal modeling approach applied to GaN devices," *IEEE Trans. Microw. Theory Techn.*, vol. 53, no. 11, pp. 3440–3448, Nov. 2005.

[9] G. Crupi, A. Caddemi, D. M. M.-P. Schreurs, and G. Dambrine, "The large world of FET small-signal equivalent circuits," *Int. J. RF Microw. Comput.-Aided Eng.*, vol. 26, no. 9, pp. 749–762, Nov. 2016.

[10] D. E. Root and B. Hughes, "Principles of nonlinear active device modeling for circuit simulation," in *32nd ARFTG Conf. Dig.*, Tempe, AZ, USA, Dec. 1988, pp. 1–24.

[11] A. Jarndal and G. Kompa, "An accurate small-signal model for AlGaN-GaN HEMT suitable for scalable large-signal model construction," *IEEE Microw. Wireless Compon. Lett.*, vol. 16, no. 6, pp. 333–335, Jun. 2006.

[12] A. Jarndal and G. Kompa, "Large-signal model for AlGaN/GaN HEMTs accurately predicts trapping and self-heating induced dispersion and intermodulation distortion," *IEEE Trans. Electron Devices*, vol. 54, no. 11, pp. 2830–2836, Nov. 2007.

[13] A. Jarndal, A. Z. Markos, and G. Kompa, "Improved modeling of GaN HEMT on Si substrate for design of RF power amplifiers," *IEEE Trans. Microw. Theory Techn.*, vol. 59, no. 3, pp. 644–651, Mar. 2011.

[14] A. Raffo *et al.*, "Nonlinear dispersive modeling of electron devices oriented to GaN power amplifier design," *IEEE Trans. Microw. Theory Techn.*, vol. 58, no. 4, pp. 710–718, Apr. 2010.

[15] X. Du *et al.*, "ANN-based large-signal model of AlGaN/GaN HEMTs with accurate buffer-related trapping effects characterization," *IEEE Trans. Microw. Theory Techn.*, vol. 68, no. 7, pp. 3090–3099, Jul. 2020.

[16] S. Lee, P. Roblin, and O. Lopez, "Modeling of distributed parasitics in power FETs," *IEEE Trans. Electron Devices*, vol. 49, no. 10, pp. 1799–1806, Oct. 2002.

[17] T. T.-L. Nguyen and S.-D. Kim, "A gate-width scalable method of parasitic parameter determination for distributed HEMT small-signal equivalent circuit," *IEEE Trans. Microw. Theory Techn.*, vol. 61, no. 10, pp. 3632–3638, Oct. 2013.

[18] G. Crupi, D. M. M.-P. Schreurs, A. Caddemi, A. Raffo, and G. Vannini, "Investigation on the non-quasi-static effect implementation for millimeter-wave FET models," *Int. J. RF Microw. Comput. Aided Eng.*, vol. 20, no. 1, pp. 87–93, Jan. 2010.

[19] G. P. Gibiino, A. Santarelli, R. Cignani, P. A. Traverso, and F. Filicori, "Measurement-based automatic extraction of FET parasitic network by linear regression," *IEEE Microw. Wireless Compon. Lett.*, vol. 29, no. 9, pp. 598–600, Sep. 2019.

[20] A. Jarndal, R. Essaadali, and A. B. Kouki, "A reliable parasitic extraction method applied to AlGaN/GaN HEMTs," *IEEE Trans. Comput.-Aided Design Integr. Circuits Syst.*, vol. 35, no. 2, pp. 211–219, Feb. 2016.

[21] A. Majumder, S. Chatterjee, S. Chatterjee, S. S. Chaudhari, and D. R. Poddar, "Optimization of small-signal model of GaN HEMT by using evolutionary algorithms," *IEEE Microw. Wireless Compon. Lett.*, vol. 27, no. 4, pp. 362–364, Apr. 2017.

[22] J. Cai, J. King, C. Yu, and L. Sun, "Bayesian inference-based small-signal modeling technique for GaN HEMTs," *Int. J. RF Microw. Comput.-Aided Eng.*, vol. 28, no. 8, e21509, Oct. 2018.

[23] A. H. Jarndal and A. S. Hussein, "Hybrid small-signal model parameter extraction of GaN HEMTs on Si and SiC substrates based on global optimization," *Int. J. RF Microw. Comput.-Aided Eng.*, vol. 29, no. 10, Oct. 2019, Art. no. e21555.

[24] J. Nocedal and S. Wright, *Numerical Optimization*, 2nd ed. New York, NY, USA: Springer, 2006.

[25] M. Locatelli and F. Schoen, *Global Optimization: Theory, Algorithms, and Applications*. Philadelphia, PA, USA: SIAM-Soc. Ind. Appl. Math., 2013.

[26] J. Kennedy and R. Eberhart, "Particle swarm optimization," in *Proc. IEEE Int. Conf. Neural Netw.*, vol. 4, 1995, pp. 1942–1948.

[27] S. Panda and N. P. Padhy, "Comparison of particle swarm optimization and genetic algorithm for FACTS-based controller design," *Appl. Soft Comput.*, vol., no. 4, pp. 1418–1427, Sep. 2008.

[28] M. Mitchell, *An Introduction to Genetic Algorithms*. Cambridge, MA, USA: MIT Press, 1998.

[29] J. Taheri, Y. Choon Lee, A. Y. Zomaya, and H. J. Siegel, "A bee colony based optimization approach for simultaneous job scheduling and data replication in grid environments," *J. Comput. Oper. Res.*, vol. 40, no. 6, pp. 1564–1578, Jun. 2013.

[30] G.-S. Hao, G.-G. Wang, Z.-J. Zhang, and D.-X. Zou, "Comparison of PSO and ABC: From A viewpoint of learning," *Trans. Comput. Sci. Eng.*, vol. 2, pp. 108–112, Nov. 2017.

[31] A. Muthiah and R. Rajkumar, "A comparison of artificial bee colony algorithm and genetic algorithm to minimize the makespan for job shop scheduling," *Procedia Eng.*, vol. 97, pp. 1745–1754, 2014.

[32] F. Filicori, G. Vannini and V. A. Monaco, "A nonlinear integral model of electron devices for HB circuit analysis," *IEEE Trans. Microw. Theory Techn.*, vol. 40, no. 7, pp. 1456–1465, Jul. 1992.

[33] A. Raffo *et al.*, "Accurate pHEMT nonlinear modeling in the presence of low-frequency dispersive effects," *IEEE Trans. Microw. Theory Techn.*, vol. 53, no. 11, pp. 3449–3459, Nov. 2005.

[34] A. Santarelli *et al.*, "Nonquasi-static large-signal model of GaN FETs through an equivalent voltage approach," *Int. J. RF Microw. Comput.-Aided Eng.*, vol. 18, no. 6, pp. 507–516, Nov. 2008.

[35] *Foundry Process Data Sheet. Ref. 170112_DS GaN GH25 Process_7012*, United Monolithic Semiconductors, Villebon-sur-Yvette, France.

[36] A. Castro, "Understand uncertainty for better test accuracy," Tech. Note, Microwave & RF, La Fox, IL, USA, Dec. 2016.

[37] R. Hassan, B. Cohanim, O. D. Weck, and G. Venter, "A comparison of particle swarm optimization and the genetic algorithm," in *Proc. 1st AIAA Multidiscipl. Design Optim. Spec. Conf.*, 2005, pp. 1–13.

[38] O. B. Augusto, S. Rabeau, P. Dépincéb, and F. Bennisb, "Multi-objective genetic algorithms: A way to improve the convergence rate," *Eng. Appl. Artif. Intell.*, vol. 19, no. 5, pp. 501–510, Aug. 2006.